Intestinal changes in permeability, tight junction and mucin synthesis in a mouse model of Alzheimer's disease

JING HE[1,2*], YUANJIE LIU[1,2*], JUNHUA LI[1,2], YUEYANG ZHAO[1,2], HANXIAO JIANG[3], SHIFANG LUO[1,2] and GUIQIONG HE[1,2]

[1]Institute of Neuroscience, [2]Department of Anatomy, School of Basic Medical Sciences, Chongqing Medical University, Chongqing 400016; [3]Department of Neurology, The Second Affiliated Hospital of Chongqing Medical University, Chongqing 400010, P.R. China

Received May 6, 2023; Accepted September 11, 2023

DOI: 10.3892/ijmm.2023.5316

Abstract. Alzheimer's disease (AD) is a neurodegenerative disorder characterized by the accumulation of amyloid-β (Aβ) in the brain. The gut/brain axis may serve a role in AD pathogenesis. The present study investigated deposition of Aβ in the intestinal epithelium and its potential effects on intestinal barrier function in a transgenic mouse model of AD. To investigate alterations in the structure and functionality of the intestinal mucosal barrier in AD model mice, hematoxylin and eosin staining for Paneth cell count, Alcian blue-periodic acid Schiff staining for goblet cells, immunohistochemistry and immunofluorescence for mucin (MUC)2 and wheat germ agglutin expression, transmission electron microscopy for mucosal ultrastructure, FITC-labeled dextran assay for intestinal permeability, quantitative PCR for goblet cell precursor expression and western blot analysis for tight junction proteins, MUC2 and inflammatory cytokine detection were performed. The results showed that AD model mice exhibited excessive Aβ deposition in the intestinal epithelium, which was accompanied by increased intestinal permeability, inflammatory changes and decreased expression of tight junction proteins. These alterations in the intestinal barrier led to an increased proliferation of goblet and Paneth cells and increased mucus synthesis. Dysfunction of gut barrier occurs in AD and may contribute to its etiology. Future therapeutic strategies to reverse AD pathology may involve early manipulation of gut physiology and its microbiota.

Correspondence to: Professor Guiqiong He or Professor Shifang Luo, Institute of Neuroscience, School of Basic Medical Sciences, Chongqing Medical University, 1 Yi Xue Yuan Road, Yuzhong, Chongqing 400016, P.R. China
E-mail: guiqionghe@cqmu.edu.cn
E-mail: 100425@cqmu.edu.cn

*Contributed equally

Abbreviations: AD, Alzheimer's disease; Aβ, amyloid-β; WT, wild-type; APP, amyloid precursor protein; PS1, presenilin 1; dTg, double transgene; LBP, lipopolysaccharide binding-protein; ZO-1, zonula occludens-1; GC, goblet cell; MUC2, mucin 2; WGA, wheat germ agglutin; PC, Paneth cell; TJ, tight junction

Key words: Alzheimer's disease, amyloid-β, intestinal barrier, goblet cell, MUC2, Notch signaling pathway

Introduction

Alzheimer's disease (AD) is a progressive neurodegenerative disease characterized by gradual cognitive loss, which is caused by the accumulation of amyloid-β (Aβ) plaques and hyper-phosphorylated τ tangles across the brain (1-3). Despite advances in AD research (4-6), the precise pathogenesis of remains obscure.

Recent studies have indicated that AD is not confined solely to the brain but extends to the gut (7,8). Patients with AD often exhibit symptoms of gastrointestinal dysfunction, inflammation and immune dysregulation (9-11). The gut/brain axis is considered to play a key role in the pathogenesis of AD (7). As the 'second brain' of the body, the gut exhibits intricate interactions with other organs, tissues and systems within the body (12). It communicates with the brain via multiple neural, endocrine and immune system pathways and can modulate behavior, mood and cognitive function by influencing neurons and synapses in the brain (13-15). Consequently, the gut is increasingly acknowledged as a vital topic of research for understanding the pathogenesis of AD (7,16).

The gut barrier comprises the epithelial layer and underlying lamina propria and serves as the first line of defense against external threats such as pathogenic bacteria and toxins (17). The epithelial layer is composed of a monolayer of polarized epithelial cells held together by tight junctions (TJs) (18). The maintenance of gut barrier integrity is regulated by various factors, including TJs, mucin (MUC) synthesis, antimicrobial peptides and immune cells (19). Recent findings suggest that disruption of the gut barrier, commonly known as 'leaky gut', is associated with various central nervous system diseases, including AD (20). A leaky gut allows gut bacteria and their products to enter the bloodstream, which activates the immune system and triggers inflammation (21); chronic inflammation is associated with the development and progression of AD (22).

Previous studies have shown that gut tissue in patients with AD undergoes changes similar to those observed in the brain tissue, such as Aβ deposition and neuronal loss (23,24). However, understanding of gut tissue alterations in patients

with AD remains limited. The present study aimed to investigate pathological changes in the gut tissue of an AD mouse model and to explore the potential involvement of the gut barrier in AD pathology. The results may offer novel insight into the pathogenesis of AD and provide promising prospects for the treatment of this condition.

Materials and methods

Animals. The double transgene (dTg) Aβ precursor protein (APP)/presenilin 1 (PS1) mice rely on an ectopic promoter to express Swedish (swe) mutations in the APP695cDNA and dE9 mutations in the PS1 gene, leading to supraphysiological levels of APP and secretion of human Aβ (25). APPswe/PS1dE9 (APP/PS1) dTg mice and non-transgenic [C57BL/6, wild-type (WT)] homologues were purchased from Institute of Biomedical Sciences, Nanjing University, Nanjing, China. The mice were housed in a room with a 12/12-h light/dark cycle, temperature controlled at 22-24˚C and humidity maintained at 50-60%. The mice had *ad libitum* access to water and food until they were 6 or 12 months old, respectively. A total of 32 male APP/PS1 mice (6- and 12-month-old; 30-38 g) and WT mice (age- and sex-matched) were used (n=8/group; Fig. 1). All experimental procedures were approved by the Ethics Committee of Chongqing Medical University (approval no. 116/2021) and followed the National Institutes of Health Guidelines for the Care and Use of Experimental Animals (26).

Intestinal permeability analysis. As previously described (27), intestinal permeability was assessed using fluorescein isothiocyanate (FITC)-dextran (4 kDa) test (Sigma-Aldrich; Merck KGaA). Briefly, mice were fasted for 4 h before receiving a 60 mg/100 g body weight oral gavage of FITC-Dextran (28). After 4 h, 200 μl of whole blood was collected from the retro-orbital venous plexus of mice deeply anesthetized with 5% isoflurane, centrifuged (4˚C) at 5,000 x g for 5 min and plasma was transferred into fresh tubes. The fluorescence intensity of FITC-dextran in separated plasma was determined using a multimode plate reader (EnSpire Plate Reader; PerkinElmer, Inc.; excitation, 485 nm; emission, 525 nm). FITC-dextran dilutions in PBS were used to obtain standard curves to calculate FITC concentration. The mice were returned to their cage after awakening from anesthesia and raised until they were sacrificed for harvesting tissue 1 week later.

Preparation of tissue. As described by Stacchiotti *et al* (29), mice were sacrificed by cervical dislocation under 5% isoflurane anesthesia. Sterile physiological saline solution (0.9% sodium chloride) was injected in the left ventricle of the heart until liver blanching. Perfused organs, including brain, ileum and proximal colon, were carefully removed.

The brain and intestinal tissue samples were rinsed with sterile saline for 1 min. The brain was divided into two halves: One half was stored at -80˚C for western blotting, while the other half was post-fixed with freshly prepared 4% paraformaldehyde (PFA) for 24 h. The ileum and proximal colon were divided equally into three segments: The first segment was fixed with 4% PFA or Carnoy's fixative (60% methanol, 30% chloroform and 10% acetic acid) for 24 h before paraffin embedding, the second segment was fixed in 2.5% glutaraldehyde for 4 h for ultrastructural investigation and the third segment was stored at -80˚C for western blotting and reverse transcription-quantitative PCR (RT-qPCR). All procedures were performed on ice.

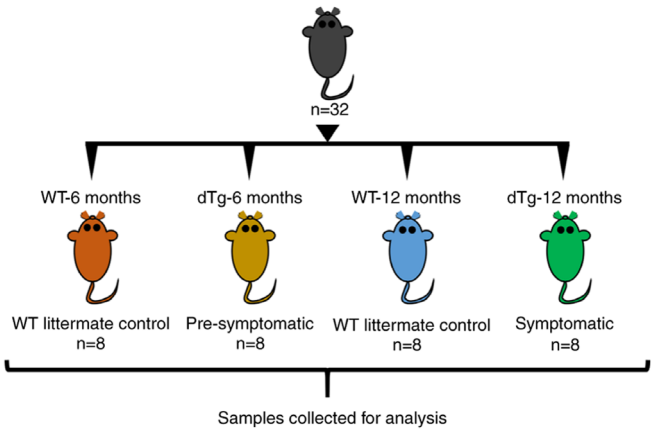

Figure 1. Timeline of pre-symptomatic animals at 6 months and symptomatic animals at 12 months. WT, wild-type; dTg, double transgene.

Hematoxylin and eosin (H&E) staining. Serial sections of paraffin-embedded ileum samples (4-μm thickness) were cut using a microtome. The paraffin sections were then deparaffinized by heating at 60˚C, washed with xylene as the deparaffinization reagent, and rehydrated through a graded series of ethanol before being stained with H&E (Beijing Solarbio Science & Technology Co., Ltd.) at room temperature for 10 min. The stained sections were observed under a light microscope (Olympus Corporation) at a magnification of x30 and images of the intestinal mucosa, villi and small intestinal epithelial cells were captured.

Alcian blue-periodic acid Schiff (AB-PAS) staining. Specimens from the ileum and proximal colon were collected and stained with AB-PAS for histochemical analysis of GCs as previously described (30). Firstly, 3-4 sections were prepared from each specimen. The sections (4-μm thick) were deparaffinized in xylene at 60˚C for 10 min and dehydrated in ethanol solution for 5 min. Oxidation of tissues was performed in 0.5% PA solution at room temperature for 5 min, followed by rinsing in distilled water. Next, sections were stained with Schiff reagent (Beijing Solarbio Science & Technology Co., Ltd.) at room temperature for 10 min and rinsed in tap water for 5 min. Subsequently, the sections were stained with 1% AB in an aqueous solution of 3% acetic acid (Ph 2.5) at room temperature for 15 min. Finally, they were counterstained with hematoxylin at room temperature for 2 min. All samples were observed under a light microscope at a magnification of x20.

Immunohistochemistry (IHC) staining. Paraffin-embedded specimens were sliced (4-μm thickness), deparaffinized in xylene at 60˚C for 10 min and hydrated in graded alcohol for 5 min each. Antigen retrieval was performed in boiling water with citric acid (pH 6.0) at 95˚C for 30 min. Endogenous peroxidase was blocked for 10 min with 3% hydrogen peroxide at 25˚C. PBS (pH 7.4) containing 5% fetal bovine serum (HyClone; Cytiva) was used to block the specimens in 0.3%

Triton X-100 for 30 min at 37˚C. Samples were incubated overnight with primary antibodies at 4˚C and then with peroxidase-conjugated anti-rabbit IgG (1:200; cat. no. MP-7451 Vector Laboratories, Inc.) at 25˚C for 30 min. Following incubation at room temperature for 30 sec with diaminobenzidine (Vector Laboratories, Inc.), the sections were rinsed with distilled water and counterstained with Mayer's hematoxylin (Vector Laboratories, Inc.) at room temperature for 2 min. The primary antibodies were mouse anti-Aβ (1: 200; cat. no. NBP2-13075; Novus Biologicals, LLC) and rabbit anti-MUC2 (1: 50; cat. no. #DF8390; Affinity Biosciences).

Immunopositivity was quantitatively evaluated using a light microscope (Olympus Corporation) at a magnification of x20. Images were analyzed using ImageJ software (version 2.1.0; National Institutes of Health) by researchers blinded to the health status of the mice and were calculated as the number of positive cells and percentage of positive area.

Immunofluorescence (IF) staining. Intestinal tissue was fixed in methanol-Carnoy and immunostained, as aforementioned. Sections were immunostained with a rabbit anti-MUC2 antibody (1:100; red; cat. no. #DF8390; Affinity Biosciences) and incubated at 4˚C overnight. Goat anti-rabbit IgG conjugated to Alexa Fluor 488 (1:1,000; cat. no. #A-11094; Thermo Fisher Scientific, Inc.) was used as the secondary antibody and applied for 1 h at room temperature. N-acetylglucosamine residues were stained with Alexa Fluor 633-labeled wheat germ agglutinin (WGA; 1:50; Novus Biologicals, LLC; green) at 37 ˚C for 30 min. Finally, sections were counterstained with DAPI (1:1,000; Sigma-Aldrich; Merck KGaA) at room temperature for 10 min.

Immunopositivity was evaluated quantitatively using a fluorescence microscope (Olympus Corporation) at x20 magnification. Images were evaluated using ImageJ software (version 2.1.0; National Institutes of Health) by researchers who were blinded to the health status of the mice and were measured as the percentage of positive area.

Transmission electron microscopy (TEM). As previously described (31), fresh intestinal tissue was removed and cut into 1.5 mm^3 pieces, which were fixed in a 2.5% glutaraldehyde solution at 4˚C for 2 h, followed by fixation in 1% osmium tetroxide at room temperature for 1 h, before being embedded in epoxy resin. Thin sections (~80 nm) were transferred onto 100 mesh copper grids and then stained with uranyl acetate at room temperature for 10 min and lead citrate for 5 min. The sections were visualized by TEM using an HT7700 device, as previously described (32).

Reverse transcription-quantitative polymerase chain reaction (RT-qPCR). RT-qPCR was conducted for specific differentially expressed genes (DEGs). The primer sequences (Table I) were designed using the online Primer3 tool (primer3.ut.ee/) for the complete coding sequences of Notch1, Hairy and enhancer of split-1 (Hes1), Mouse atonal homolog 1 (Math1), Growth factor independence 1 (Gfi1), SAM pointed domain-containing ETS transcription factor (spdef), Kinesin family member 4 (Kif4), and β-actin. These sequences were obtained from the NCBI Genbank (ncbi.nlm.nih.gov) database. Primer specificity was confirmed using the Primer-BLAST tool (blast.ncbi.nlm.nih.gov/Blast.cgi), and the primers were synthesized by Beijing Tsingke Biotech Co., Ltd. For RT-qPCR, total RNA was extracted from proximal colonic tissue using TRIzol® (cat. no. #9108; Takara Biotechnology Co., Ltd.). RT was carried out using the PrimeScript™ RT Master Mix according to the manufacturer's protocol (cat. no. #RR037A; Takara Biotechnology Co., Ltd.) to synthesize cDNA. Subsequently, SYBR Premix Ex Taq™ (cat. no. #RR820A; Takara Biotechnology Co., Ltd.) was used to perform qPCR to assess changes in gene expression. The qPCR thermal cycling conditions were as follows: an initial denaturation step at 95˚C for 30 sec, followed by 40 cycles of denaturation at 95˚C for 5 sec and annealing/extension at 60˚C for 30 sec. Each sample was subjected to PCR amplification in triplicate. The $2^{-\Delta\Delta Cq}$ method (33) was employed to normalize the RNA expression levels of genes against β-actin.

Western blot analysis. Proteins were extracted using RIPA lysis buffer and protease inhibitor (both Beijing Solarbio Science & Technology Co., Ltd.). Protein concentration was measured with a BCA Protein Detection kit (Beijing Solarbio Science & Technology Co., Ltd.). Equal quantities of protein (20 μg/lane) were separated by 10% SDS-PAGE and transferred to PVDF membranes. The membranes were blocked with 5% skimmed milk at room temperature for 2 h and incubated with primary antibodies (Table II) at 4˚C overnight, followed by incubation with horseradish peroxidase-conjugated secondary antibodies (goat anti-mouse, cat. no. S0002, or anti-rabbit IgG, cat. no. S0001, both Affinity Biosciences) for 1 h at 25˚C. The membranes were finally visualized using immobilon forte western HRP substrate (MilliporeSigma). The intensity of the signal was evaluated by densitometry using ImageJ (version 2.1.0; National Institutes of Health), and the value was normalized to the loading control (α-tubulin).

Statistical analysis. Data are presented as the mean ± SEM from three or more independent experiments. GraphPad Prism 6 software (GraphPad Software, Inc.; Dotmatics) was used for all analyses. Data were compared using unpaired Student's t test or two-way ANOVA followed by Bonferroni's post hoc test. $P<0.05$ was considered to indicate a statistically significant difference.

Results

Increased Aβ immunoreactivity in brain and intestine of dTg mice. The present study first examined Aβ immunoreactivity and expression of its substrate APP and limiting enzyme β-secretase 1 (BACE1) in the brain of dTg mice and their WT counterparts. Senile plaques (SP) in the cortex and hippocampus were detected by immunohistochemical staining with anti-Aβ antibodies. IHC showed that Aβ-positive plaques were only observed in dTg mice. More plaques were observed in the cortex and hippocampus in 12-month than in 6-month dTg mice. No plaques were observed in the brain of WT mice (Fig. 2A and B). Western blotting showed that APP protein was overexpressed in the brain of both 6 and 12-month dTg compared with WT mice. Accordingly, the expression of BACE1 protein was significantly increased in the brain of both groups of dTg mice (Fig. 2C-E).

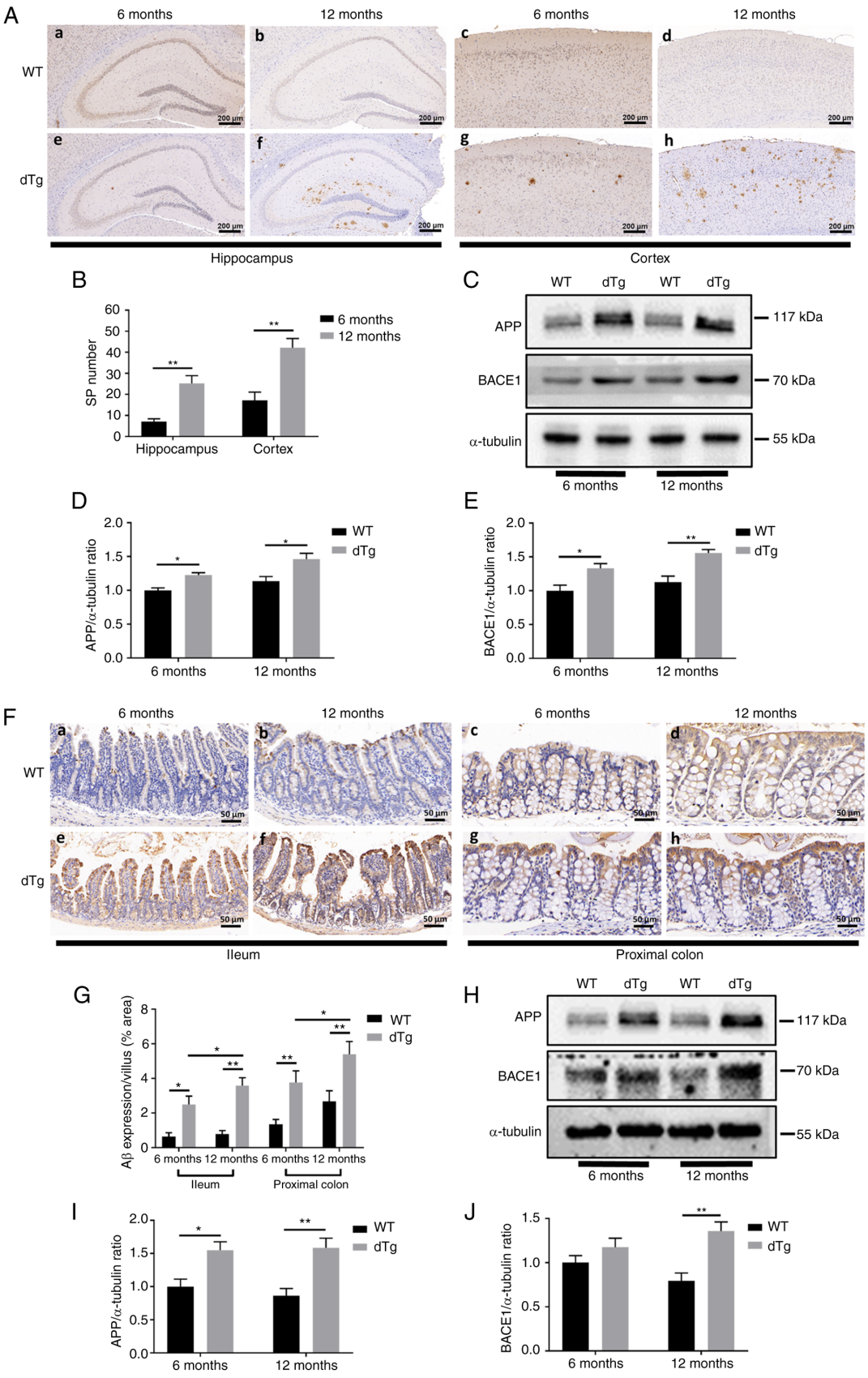

Figure 2. SP deposition in cortex and hippocampus and Aβ aggregation in intestinal mucosa. Immunohistochemistry showed SP in (Aa-h) cortex and hippocampus of WT and dTg mice at 6 and 12 months, respectively. (B) The number of SP were determined by immunohistochemistry in the cortex and hippocampus (scale bar, 200 μm; n=6/group). (C) Protein levels of APP and BACE1 in extracts of cortex and hippocampus tissue were detected by western blotting. Western blot quantification of (D) APP and (E) BACE1 (n=4/group). Immunohistochemistry showed Aβ aggregation in (Fa-h) intestinal mucosa of WT and dTg mice at 6 and 12 months, respectively. (G) Aβ expression area were determined by immunohistochemistry in ileum and proximal colon (scale bar, 50 μm; n=6/group). (H) Protein levels of APP and BACE1 in extracts of intestinal tissue were detected by western blotting. Western blot quantification of (I) APP and (J) BACE1 (n=4/group). *P<0.05, **P<0.01. SP, senile plaque; Aβ, amyloid-β; dTg, double transgene; WT, wild-type; APP, amyloid precursor protein; BACE1, β site APP cleaving enzyme 1.

Table I. Primer sequences.

Gene	Forward, (5'-3')	Reverse (5'-3')	Accession no.
β-actin	GGCTCCTAGCACCATGAAGA	AAAACGCAGCTCAGTAACAGT	NM_007393.5
Notch1	CCCGCTGTGAGATTGATGTTAAT	ACACCTTCATAACCTGGCATACA	NM_008714.3
Hes1	GGCAGACATTCTGGAAATGA	TTGATCTGGGTCATGCAGTT	NM_001416728.1
Math1	GAGTGGGCTGAGGTAAAAGAGT	GGTCGGTGCTATCCAGGAG	NM_061763.5
Gfi1	ATCAAATGCAGCAAGGTGTTCTC	GTGTCCGAGTGAATGAGCAGATG	NM_010278.2
Spdef	CTGGGAGCACGTTGGATGAG	CGGTACTGGTGTTCTGTCCA	NM_001414277.1
Kif4	CTCGAAGCCAAATGTGCCATAAA	TCCACTTTGACCAGCTCTTCTTT	NM_008446.3

Hes1, Hairy and enhancer of split-1; Math1, Mouse atonal homolog 1; Gfi1, Growth factor independence 1; Spdef, SAM pointed domain-containing ETS transcription factor; Kif4, Kinesin family member 4.

Table II. Monoclonal primary antibodies in western blotting.

Antibody	Source	Cat. no.	Manufacturer	Dilution
APP	Rabbit	#29765	CST	1:1,000
BACE1	Rabbit	#5606	CST	1:1,000
MUC2	Rabbit	#DF8390	Affinity Biosciences	1:1,000
ZO-1	Rabbit	ab276131	Abcam	1:1,000
Occludin	Rabbit	ab216327	Abcam	1:1,000
Claudin1	Rabbit	ab180158	Abcam	1:2,000
LBP	Rabbit	ab254559	Abcam	1:1,000
IL1β	Rabbit	ab254360	Abcam	1:1,000
TNFα	Rabbit	ab183218	Abcam	1:1,000
α-tubulin	Mouse	ab7291	Abcam	1:10,000

APP, amyloid precursor protein; BACE1, beta-site APP cleaving enzyme 1; MUC2, mucin 2; ZO-1, zonula occludens-1; LBP, lipopolysaccharide binding-protein; CST, Cell Signaling Technology, Inc.

Aβ immunoreactivity was examined in the ileum and proximal colon. The results showed higher Aβ levels in dTg compared with WT mice, and Aβ-positive expression was more pronounced in the 12- than in the 6-month group, which was consistent with observations in the cortex and hippocampus. Aβ expression was significantly increased in dTg compared with WT mice of the same age (Fig. 2F and G). Western blotting revealed overexpression of APP in the 6- and 12-month dTg groups compared with WT mice, while BACE1 expression was significantly higher only in the 12-month dTg group (Fig. 2H-J). These results indicated pathological changes in the gut of AD model mice, similar to those in AD brain.

Increased intestinal permeability in dTg mice. To investigate whether increased intestinal Aβ exerted an effect on the intestinal barrier, an intestinal permeability assay was performed. The variation in epithelial permeability was measured by FITC-dextran assay. Compared with WT, dTg mice showed a significant increase in intestinal mucosal permeability in 6- and 12-month groups, respectively. Furthermore, intestinal permeability of 12-month dTg mice was significantly higher than that of 6-month dTg mice (Fig. 3).

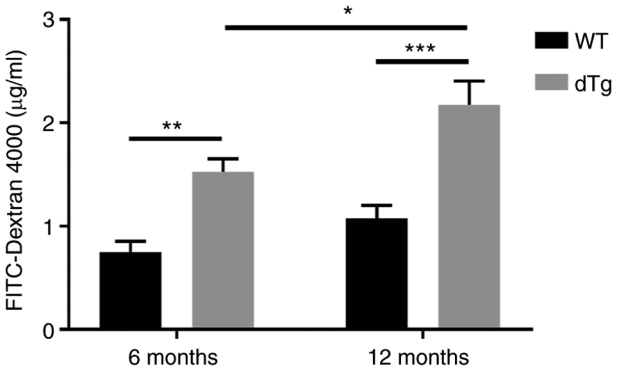

Figure 3. Variation in intestinal permeability. Intestinal permeability assays were conducted with FITC-dextran (n=4/group). *P<0.05, **P<0.01, ***P<0.001. WT, wild-type; dTg, double transgene.

Elevated lipopolysaccharide-binding protein (LBP) and cytokine protein expression in dTg mice. Increased intestinal permeability can lead to susceptibility to inflammation (34). To evaluate intestinal inflammation, the present study measured LBP, IL1β and TNFα protein expression in intestinal tissue, which play crucial roles in mediating

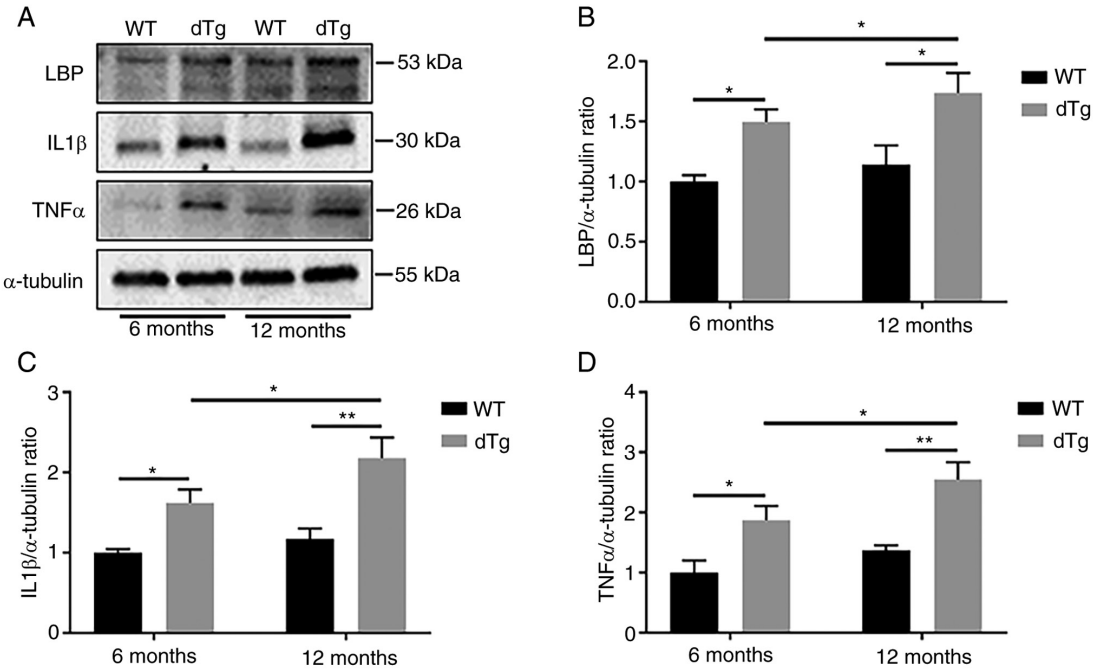

Figure 4. Variation in inflammatory indicators of the intestine. (A) Protein levels of LBP, IL-1β and TNFα in extracts of intestine tissue were detected by western blotting. Western blot quantification of (B) LBP, (C) IL-1β and (D) TNF-α (n=4/group). *P<0.05, **P<0.01. LBP, lipopolysaccharide binding-protein; WT, wild-type; dTg, double transgene.

inflammatory and anti-inflammatory responses (35-37). Notably, dTg mice exhibited significantly higher LBP protein expression at 6 and 12 months compared with their WT counterparts. Additionally, dTg mice displayed increased production of proinflammatory cytokines (IL-1β and TNFα) in the 6- and 12-month groups compared with WT mice. Furthermore, expression levels of LBP, IL1β and TNFα were significantly elevated in the 12-month dTg mice compared with the 6-month group (Fig. 4A-D).

Damaged intestinal epithelial TJ in dTg mice. The disruption of TJs in intestinal epithelium, which is associated with intestinal inflammation (38), was examined using TEM images to show the ultrastructure of the ileum and proximal colon mucosa (Fig. 5A). WT mice had normal intestinal epithelial morphology with uniform distribution of microvilli, tight cell junctions and normal organelle morphology (Fig. 5Aa-d). However, intestinal epithelial integrity was disrupted in all dTg mice, which was evidenced by microvilli breakage or absence, TJ damage and bacterial invasion (Fig. 5Ae-h).

The protein expression of zonula occludens-1 (ZO-1), occludin, and claudin 1 in proximal colon was analyzed using western blotting. The expression of these proteins was significantly decreased in both 6- and 12-month dTg mice compared with their WT counterparts. Additionally, expression of ZO-1, occludin and claudin 1 was lower in the 12-month group of dTg mice compared with the 6-month group (Fig. 5B-E).

Increased number of goblet cells (GCs) and elevated expression and glycosylation of MUC2 in dTg mouse intestine. Mucus, which is synthesized by GCs, is an essential component of the intestinal barrier (39). To investigate the impact of Aβ on GCs, AB-PAS staining was conducted to evaluate the quantity and morphology of GCs. The results showed a significant increase in number of GCs in the ileum and proximal colon of dTg mice at 6 and 12 months compared with WT mice. Notably, GCs in the 12-month group of dTg mice were significantly decreased compared with the 6-month group of dTg mice in the proximal colon (Fig. 6A and C). Similar results were observed in the analysis of Paneth cells (PCs; Fig. S1A and B). Compared with WT mice, dTg mice had significantly increased PCs in the ileum at 6 and 12 months. PCs in the ileum of 12-month group of dTg mice were significantly reduced compared with 6-month group of dTg mice.

The present study assessed whether changes in GCs affected MUC synthesis by immunostaining GCs with specific markers such as MUC2. In both the ileum and proximal colon, the area of MUC2-positive cells in the crypts of dTg mice were significantly increased compared with those in WT mice at 6 and 12 months. Notably, expression of MUC2 was significantly reduced in 12- compared with 6-month dTg mice (Fig. 6B and D). Consistent with the IHC staining, compared with WT mice, protein expression of MUC2 was elevated in the 6- and 12-month groups of dTg mice, while the 12-month dTg mice had significantly lower expression than the 6-month group in the proximal colon (Fig. 6E and F).

To evaluate the function of mucus as a barrier, the present study assessed MUC glycosylation using IF staining with anti-MUC2 antibody and WGA lectin in the ileum and proximal colon. MUC2 was glycosylated and confined to GCs in intestinal mucosa. IF staining revealed a significant increase in MUC2 in dTg compared with WT mice in both the ileum and proximal colon at 6 and 12 months, while 12-month dTg mice had lower expression than 6-month dTg mice. WGA staining also showed similar results. WGA expression in ileum and proximal colon of 6- and 12-month dTg mice was significantly increased compared with WT mice, while WGA expression in 12-month dTg mice was significantly lower than in 6-month

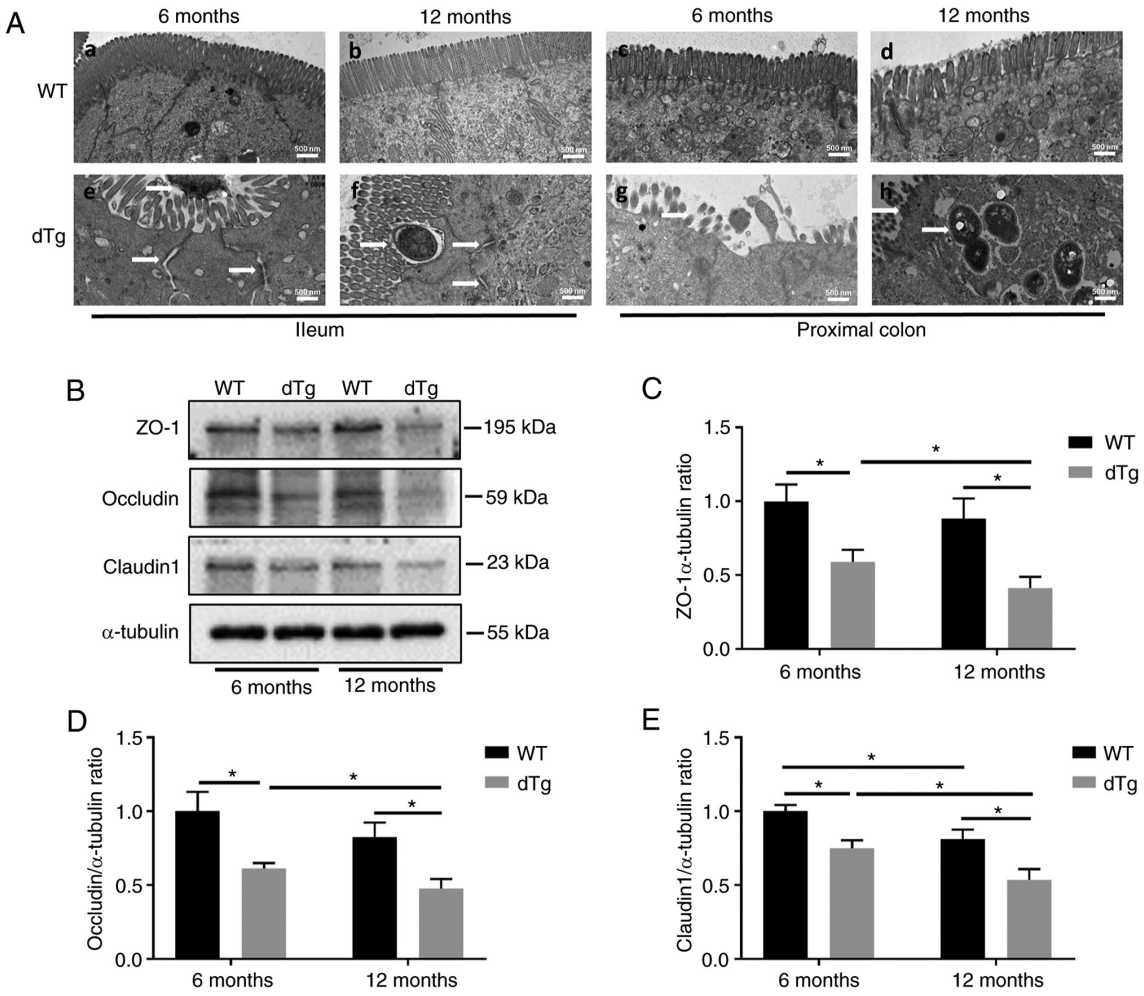

Figure 5. Variation in ultrastructure of intestinal mucosa. Electron micrograph images of ileum and proximal colonic segments harvested from WT and dTg mice at 6 and 12 months. (Ae-h) Abnormal intestinal microvilli, tight junctions and flora invasion in dTg mice (white arrows). (B) Levels of (C) ZO-1, (D) occludin, (E) claudin-1 and GAPDH in extracts of intestinal tissue were detected by western blotting (n=4/group). *P<0.05. dTg, double transgene; WT, wild-type; ZO-1, zona occludens-1.

dTg mice. In addition, O-glycosylation was most abundant in GCs at the bottom of intestinal crypts and on the mucosal surface of the intestine (Fig. 7A-F).

Disrupted Notch signaling and GC differentiation markers in intestine of dTg mice. GCs were increased in dTg mice. Notch signaling is known to regulate stem cell fate determination in crypts via Notch1. Upon activation, Notch1 promotes the expression of Hes-1, which in turn suppresses Math1 downstream, leading to increased enterocytes and decreased differentiation into GCs and expression of MUC2 (40). Therefore, the present study examined the status of Notch signaling. RT-qPCR analysis (Fig. 8) revealed that the mRNA levels of Notch1 and Hes-1 were significantly decreased in proximal colon of 6- and 12-month dTg mice compared with WT mice, while levels of downstream Math1, Gfi1, Spdef and Klf4 were increased in 6- and 12-month dTg compared with WT mice.

Discussion

Transgenic mouse models of AD provide a useful tool for studying pathogenesis of AD, as well as novel therapeutic interventions. The first mouse models of AD were based on transgenic expression of human APP and exhibited robust amyloid pathology and memory deficits, but most of these models need at least 10 months to develop SP or exhibit learning and memory deficits. Singly transgenic human presenilin 1 (PS1) or PS2 mutant mice do not develop AD pathology or cognitive deficit, although they increase Aβ42 levels with no effect on Aβ40. The most widely used APP/PS1 mouse model was developed through co-injecting the APP and PS1 transgenes. APP/PS1 created by David Borchelt combines human APP containing the swe mutation and PS1 containing e δE9 mutation (41). Amyloid plaques begin to appear in the mouse cortex ~4 months and in the hippocampus ~6 months, and they increase in size and number with age. Deficits in learning and memory arise between 6 and 10 months and worsen with age (42,43).

The intestinal barrier consists of cellular and extracellular elements (44). Intestinal epithelial cells constitute the primary cellular element of the intestinal barrier and are interconnected by junctional complexes. The barrier permits uptake of nutrients, electrolytes and water, while constituting a defense against intraluminal toxins, antigens and enteric flora (45,46). TJs are a fundamental junctional complex

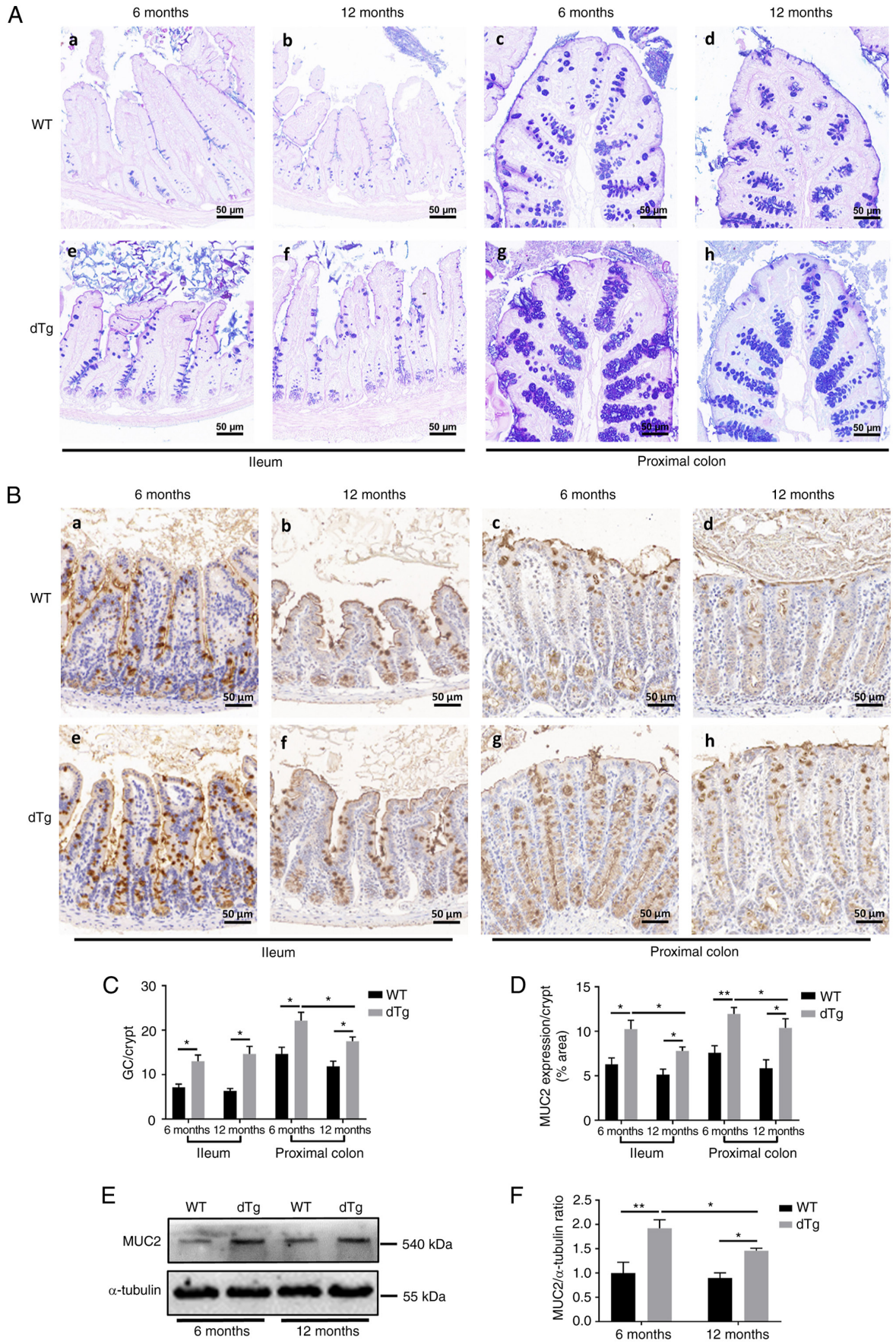

Figure 6. Variation in number of GCs and MUC2 expression in intestinal mucosa. (Aa-h) Alcian blue-Periodic acid Schiff staining showed GCs and (Ba-h) immunohistochemistry showed MUC2 in the ileum and proximal colon of WT and dTg mice at 6 and 12 months. (C) Number of GCs, as determined by histochemical staining of the ileum and proximal colon. (D) MUC2 expression area in the ileum and proximal colon was determined by immunohistochemistry (n=6/group). Scale bar, 50 μm. (E) Protein levels of MUC2 in extracts of intestinal tissue were detected by western blotting. (F) Quantification of the western blot results (n=4/group). *P<0.05, **P<0.01. GC, goblet cell; WT, wild-type; dTg, double transgene; MUC2, mucin 2; WGA, wheat germ agglutin.

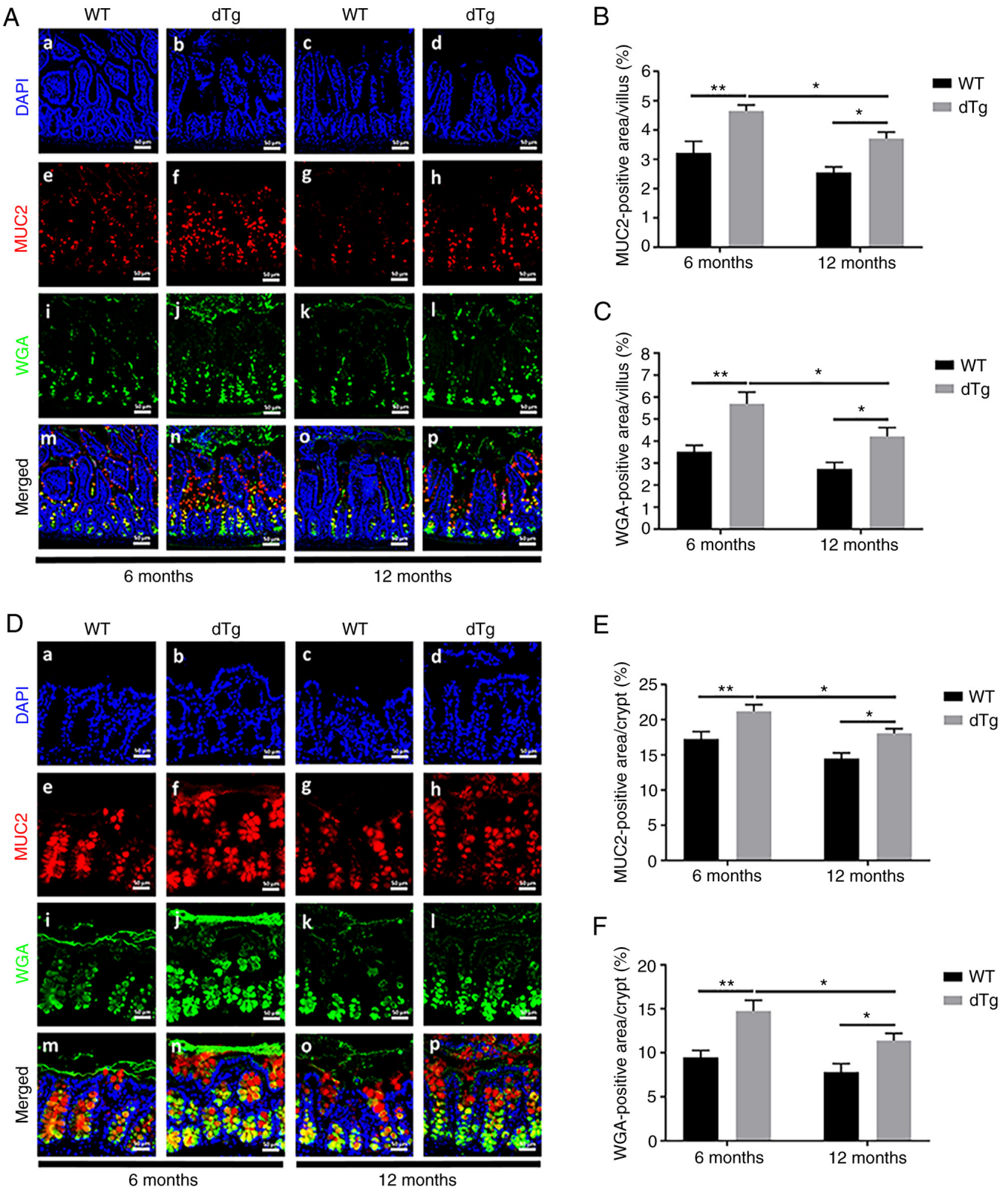

Figure 7. Variation in MUC2 and WGA in intestinal mucosa. (Aa-p) IF showed MUC2 and WGA in ileum of WT and dTg mice at 6 and 12 months. (B) MUC2- and (C) WGA-positive area was determined by IF in ileum (n=6/group). IF showed MUC2 and WGA in (Da-p) proximal colon of WT and dTg mice at 6 and 12 months. (E) MUC2- and (F) WGA-positive area was determined by IF in proximal colon (n=6/group). *P<0.05, **P<0.01. WGA, wheat germ agglutinin; IF, immunofluorescence; MUC2, mucin 2; WT, wild-type; dTg, double transgene.

consisting of TJ proteins, including transmembrane proteins such as claudin-1 and occludin, and the peripheral membrane adaptor protein ZO-1, which serves a vital role in preserving the integrity of the intestinal barrier and regulating intestinal permeability (47). The loss of TJ proteins increases intestinal permeability (48). In the present study, intestinal concentrations

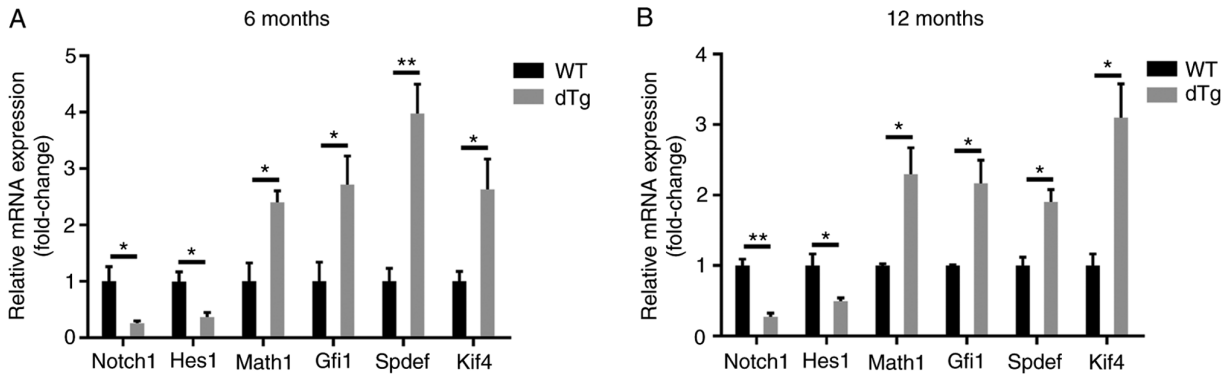

Figure 8. Differentiation function of GCs in intestinal mucosa. The expression of GC markers was quantified by reverse transcription-quantitative PCR (n=3/group). *P<0.05, **P<0.01. GC, goblet cell; WT, wild-type; dTg, double transgene; Hes1, Hairy and enhancer of split-1; Math1, Mouse atonal homolog 1; Gfi1, Growth factor independence 1; Spdef, SAM pointed domain-containing ETS transcription factor; Kif4, Kinesin family member 4.

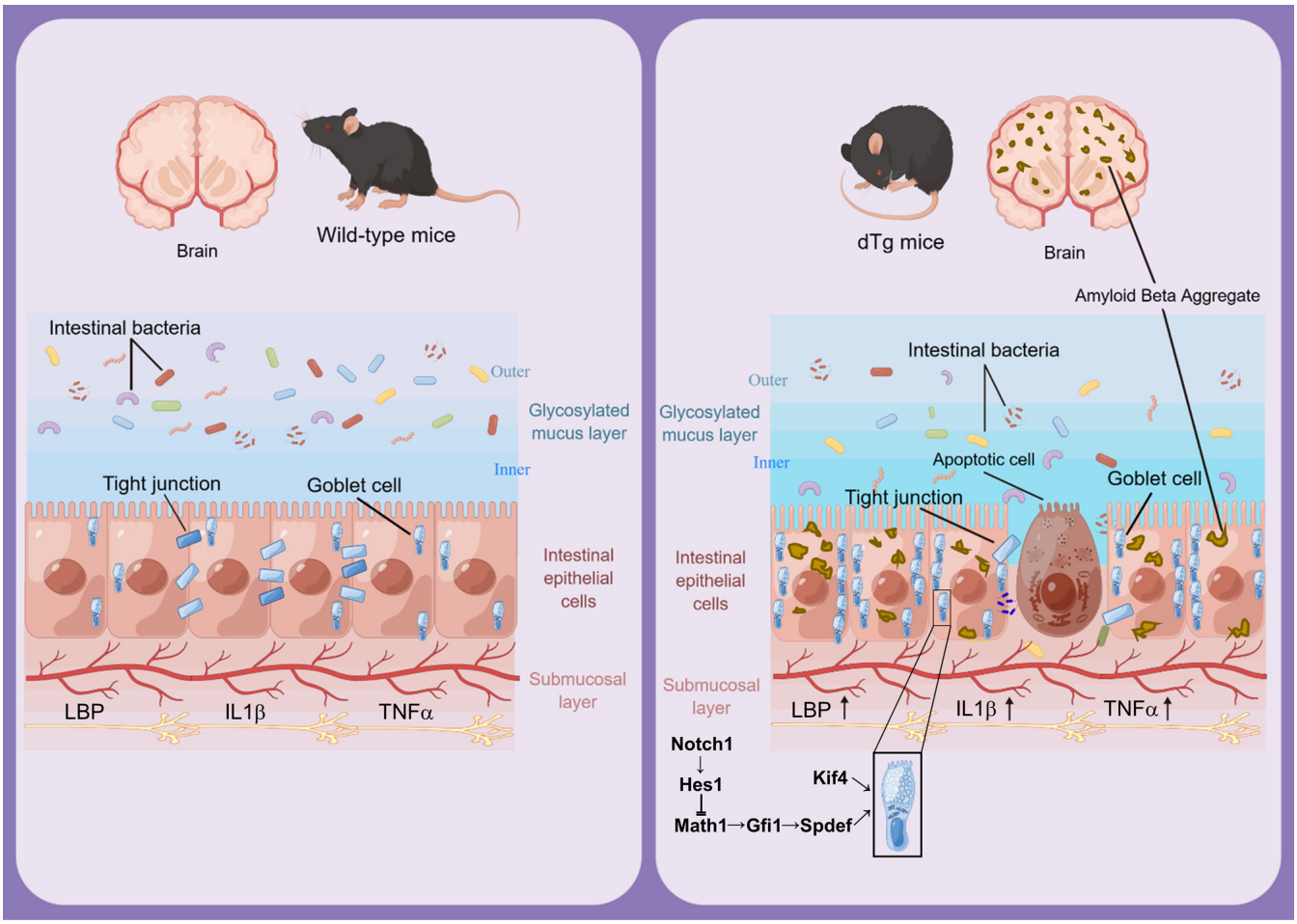

Figure 9. Schematic representation of brain and intestinal variation between wild-type and dTg mice. Alzheimer's disease model dTg mice exhibited aggregation of amyloid plaques in both the brain and intestinal epithelium, increased intestinal permeability, elevated levels of lipopolysaccharide-binding protein, IL-1β and TNFα, decreased tight junction proteins, bacterial infiltration into the intestinal epithelium and increased goblet cell count and mucus synthesis. dTg, double transgene; LBP, lipopolysaccharide-binding-protein; Math1, Mouse atonal homolog 1; Gfi1, Growth factor independence 1; Spdef, SAM pointed domain-containing ETS transcription factor; Kif4, Kinesin family member 4.

of ZO-1, occludin, and claudin-1 were significantly decreased in dTg mice. Ultrastructural alterations, including microvilli breakage and absence, TJ damage and bacterial invasion, were demonstrated by TEM. Overall, these observations suggested disruption of barrier integrity in dTg mice, which exhibited greater intestinal permeability. This increase in intestinal permeability was confirmed by FITC-dextran assay in both the ileum and proximal colon mucosa of dTg mice.

Inflammatory-induced intestinal barrier dysfunction is a key factor in regulating intestinal permeability. Chronic low-grade enteric inflammation causes alterations and/or disassembly of intercellular junctions, which contribute to

severe pathological alterations of the intestinal wall and intestinal barrier dysfunction (49). Significantly elevated LBP, IL-1β and TNFα in intestinal tissue of 6-month-old dTg mice suggested the presence of an inflammatory response in the early stages of AD and the inflammatory response increased with the progression of AD. The inflammatory response interferes with TJs and increases intestinal permeability due to dysregulation of TJ protein expression (50). Furthermore, the present data showed positive immunoreactivity for Aβ in the intestinal epithelium, suggesting immune and inflammatory responses. However, Aβ is an inflammatory stimulator as well as a peptide at the center of AD that triggers inflammatory alterations and releases strong neurotoxic products such as oxygen-free radicals, chemokines, cytokines and other inflammatory proteins (51-53). Additionally, a significant increase in PC count was also observed in dTg mice. PCs are critical for regulating immune responses and resisting microbial invasion by releasing antimicrobial peptides (54).

The extracellular environment of the intestine comprises mucus serving as a protective barrier, enzymes involved in digestion, immune cells and cytokines participating in immune responses, as well as nutrients, waste products, and microorganisms, among others. (55-57) These extracellular components contribute to the complex and dynamic environment of the intestinal tract. Among the extracellular components, MUC2, which is a typical secretory gel-forming MUC produced by GCs, is highly expressed in the colon with lower levels in the small intestine (58). Before secretion, glycosylated MUC2 is densely packed and stored in secretory GC vesicles. MUC2 contains several O-linked saccharidic chains and MUC-type O-glycans are key factors in protecting the intestinal mucus barrier from damage (59). Lectins linked to fluorescein were used as carbohydrate probes to detect the primary residuals in the oligosaccharidic chains of the GC MUC (60). FITC-WGA recognizes the residues both of N-Acetylglucosamine and sialic acid (61). The present results showed increased amounts of glycosylated residues in the dTg mice, which was consistent with the upregulation of MUC2 synthesis observed in the dTg mice. However, the amount and glycosylation pattern of MUC2 reduced in 12-compared with 6-month dTg mice, potentially indicating mucosal barrier impairment after prolonged stimulation. This may be due to prolonged mucosal glycosylation burden, leading to gradual fatigue of the glycosylation system and decline in MUC2 glycosylation. Furthermore, there were differences in morphology of MUC2 and WGA between GCs of ileum and those of proximal colon. However, further investigations are needed. The present study showed mucous metaplasia in the proximal colonic epithelium of dTg mice, with an increased number of GCs filled with acid and heterochromatic MUC. MUC and mucinous metaplasia were increased presence in response to the rapid turnover of epithelial cells within proximal colonic crypts. The Notch signaling pathway is associated with GC proliferation (40). Notch1 and Hes-1 are expressed in intestinal crypts, and further analysis of Hes-1 and Math1 [which are Notch targets and downstream effectors (62,63)], indicated a role of Notch signaling in regulating the development and homeostasis of intestinal epithelia. In secretory lineages, such as GCs, Hes-1 directly binds to the Math1 transcription factor, leading to decreased Math1 expression and downstream Gfi1, Spdef and Klf4 (64-67). The present data suggested that GCs were upregulated in dTg mice by suppressing Notch signaling and increasing differentiation of Intestinal Stem Cells to form goblets, enhancing mucus and MUC formation. Here, protein levels of MUC2 were significantly increased in proximal colonic tissue. In light of the single effect of Notch signaling on mucus and GCs, Notch signaling was aberrantly inhibited in dTg mice. The present results suggested that dTg mouse mucosa may compensate for MUC2 and GC proliferation by inhibiting the Notch signaling pathway, thereby strengthening the mucus barrier. In addition, claudin-1 is a key component of the TJ complex; however, research has suggested other potential functions of claudin-1 (68). Claudin-1 modifies intestinal epithelial homeostasis via Notch-signaling regulation. Upregulated expression of claudin-1 induces MMP-9 and phosphorylated-ERK signaling to activate Notch signaling, which inhibits the differentiation of GCs, thus decreasing the number of GCs and MUC2 expression (69). However, downregulation of claudin-1 causes an increase in GC number (70), which remains to be confirmed in dTg mouse intestines. Mucus secretion increased with GC number in the present study, which may result from the inflammatory response in the intestine. This suggested that the increased proliferative activity of GCs may be a protective mechanism to strengthen the intestinal barrier. However, over time, this protective mechanism weakened. The present study further confirmed that in AD model mice, there was an overabundance of Aβ accumulation within the intestinal epithelium. This was accompanied by heightened permeability, inflammation-related alterations, and a reduction in tight junction (TJ) proteins. These changes led to heightened reactive proliferation of goblet cells (GCs), along with an increase in the production of mucus (Fig. 9).

In summary, the present study demonstrated that intestinal changes in permeability, TJ and mucin synthesis in a mouse model of AD. The present findings may provide novel insight into the pathogenesis of AD and potential options for the treatment of this disease. Furthermore, the present findings warrant further investigation to elucidate the mechanisms responsible for the interaction between intestinal Aβ deposition and gut barrier disruption in AD.

Acknowledgements

Not applicable.

Funding

The present study was supported by Scientific and Technological Research Program of Chongqing Municipal Education Commission (grant nos. KJCXZD2020021 and KJZD-K201900403), Chongqing Medical University Program for Youth Innovation in Future Medicine (grant no. W0044) and General Project of Chongqing Natural Science Foundation (grant no. cstc2021jcyj-msxmX0442).

Availability of data and materials

The datasets used and/or analyzed during the current study are available from the corresponding author on reasonable request.

Authors' contributions

GH and SL conceived and designed the study. JH and YL performed the experiments and drafted the manuscript, YZ, HJ and JL conducted the statistical analysis. GH, SL, YL and JH confirm the authenticity of all the raw data. All authors have read and approved the final manuscript.

Ethics approval and consent to participate

All procedures involving animals were performed under institutional guidelines. The present study was approved by The Ethics Committee of Chongqing Medical University (approval no. 116/2021).

Patient consent for publication

Not applicable.

Competing interests

The authors declare that they have no competing interests.

References

1. Lane CA, Hardy J and Schott JM: Alzheimer's disease. Eur J Neurol 25: 59-70, 2018.
2. Soria Lopez JA, Gonzalez HM and Leger GC: Alzheimer's disease. Handb Clin Neurol. 167: 231-55, 2019.
3. Sun BL, Li WW, Zhu C, Jin WS, Zeng F, Liu YH, Bu XL, Zhu J, Yao XQ and Wang YJ: Clinical Research on Alzheimer's Disease: Progress and Perspectives. Neurosci Bull 34: 1111-1118, 2018.
4. Monteiro AR, Barbosa DJ, Remiao F and Silva R: Alzheimer's disease: Insights and new prospects in disease pathophysiology, biomarkers and disease-modifying drugs. Biochem Pharmacol 211: 115522, 2023.
5. Cervellati C and Zuliani G: Frontier on Alzheimer's Disease. Int J Mol Sci 24: 7748, 2023.
6. Wood PL: Failure of current Alzheimer's disease hypotheses. Aging (Albany NY) 15: 5959-560, 2023.
7. Jin J, Xu Z, Zhang L, Zhang C, Zhao X, Mao Y, Zhang H, Liang X, Wu J, Yang Y and Zhang J: Gut-derived β-amyloid: Likely a centerpiece of the gut-brain axis contributing to Alzheimer's pathogenesis. Gut Microbes 15: 2167172, 2023.
8. Chen C, Zhou Y, Wang H, Alam A, Kang SS, Ahn EH, Liu X, Jia J and Ye K: Gut inflammation triggers C/EBPβ/δ-secretase-dependent gut-to-brain propagation of Aβ and Tau fibrils in Alzheimer's disease. EMBO J 40: e106320, 2021.
9. Wang D, Zhang X and Du H: Inflammatory bowel disease: A potential pathogenic factor of Alzheimer's disease. Prog Neuropsychopharmacol Biol Psychiatry 119: 110610, 2022.
10. Eiser AR and Fulop T: Alzheimer's Disease Is a Multi-Organ Disorder: It may already be preventable. J Alzheimers Dis 91: 1277-1281, 2023.
11. MahmoudianDehkordi S, Arnold M, Nho K, Ahmad S, Jia W, Xie G, Louie G, Kueider-Paisley A, Moseley MA, Thompson JW, *et al*: Altered bile acid profile associates with cognitive impairment in Alzheimer's disease-An emerging role for gut microbiome. Alzheimers Dement 15: 76-92, 2019.
12. Dupont HL, Jiang ZD, Dupont AW and Utay NS: The intestinal microbiome in human health and disease. Trans Am Clin Climatol Assoc 131: 178-197, 2020.
13. De la Fuente M: The Role of the Microbiota-Gut-Brain axis in the health and illness condition: A focus on Alzheimer's disease. J Alzheimers Dis 81: 1345-160, 2021.
14. Kesika P, Suganthy N, Sivamaruthi BS and Chaiyasut CL: Role of gut-brain axis, gut microbial composition, and probiotic intervention in Alzheimer's disease. Life Sci 264: 118627, 2021.
15. Glinert A, Turjeman S, Elliott E and Koren O: Microbes, metabolites and (synaptic) malleability, oh my! The effect of the microbiome on synaptic plasticity. Biol Rev Camb Philos Soc 97: 582-599, 2022.
16. Nafady MH, Sayed ZS, Abdelkawy DA, Shebl ME, Elsayed RA, Ashraf GM, Perveen A, Attia MS and Bahbah EI: The effect of gut microbe dysbiosis on the pathogenesis of Alzheimer's Disease (AD) and related conditions. Curr Alzheimer Res 19: 274-284, 2022.
17. Liu L, Yin M, Gao J, Yu C, Lin J, Wu A, Zhu J, Xu C and Liu X: Intestinal barrier function in the pathogenesis of nonalcoholic fatty liver disease. J Clin Transl Hepatol 11: 452-458, 2023.
18. Jia J, Zheng W, Zhang C, Zhang P, Guo X, Song S and Ai C: Fucoidan from Scytosiphon lomentaria protects against destruction of intestinal barrier, inflammation and lipid abnormality by modulating the gut microbiota in dietary fibers-deficient mice. Int J Biol Macromol 224: 556-567, 2023.
19. Srugo SA, Bloise E, Nguyen TTN and Connor KL: Impact of maternal malnutrition on gut barrier defense: Implications for pregnancy health and fetal development. Nutrients 11: 1375, 2019.
20. Neri I, Boschetti E, Follo MY, De Giorgio R, Cocco LI, Manzoli L and Ratti S: Microbiota-Gut-Brain axis in neurological disorders: From leaky barriers microanatomical changes to biochemical processes. Mini Rev Med Chem 23: 307-319, 2023.
21. El-Hakim Y, Bake S, Mani KK and Sohrabji F: Impact of intestinal disorders on central and peripheral nervous system diseases. Neurobiol Dis 165: 105627, 2022.
22. Oh E, Kang JH, Jo KW, Shin WS, Jeong YH, Kang B, Rho TY, Jeon SY, Lee J, Song IS and Kim KT: Synthetic PPAR Agonist DTMB Alleviates Alzheimer's disease pathology by inhibition of chronic microglial inflammation in 5xFAD Mice. Neurotherapeutics 19: 1546-1565, 2022.
23. Manocha GD, Floden AM, Miller NM, Smith AJ, Nagamoto-Combs K, Saito T, Saido TC and Combs CK: Temporal progression of Alzheimer's disease in brains and intestines of transgenic mice. Neurobiol Aging 81: 166-176, 2019.
24. Puig KL, Lutz BM, Urquhart SA, Rebel AA, Zhou X, Manocha GD, Sens M, Tuteja AK, Foster NL and Combs CK: Overexpression of mutant amyloid-beta protein precursor and presenilin 1 modulates enteric nervous system. J Alzheimers Dis 44: 1263-1278, 2015.
25. Niidome T, Taniuchi N, Akaike A, Kihara T and Sugimoto H: Differential regulation of neurogenesis in two neurogenic regions of APPswe/PS1dE9 transgenic mice. Neuroreport 19: 1361-1364, 2008.
26. National Research Council (US) Committee for the Update of the Guide for the Care and Use of Laboratory Animals: Guide for the Care and Use of Laboratory Animals, 8th edition. National Academies Press (US), Washington, DC, 2011.
27. Nakanishi T, Fukui H, Wang X, Nishiumi S, Yokota H, Makizaki Y, Tanaka Y, Ohno H, Tomita T, Oshima T and Miwa H: Effect of a High-Fat Diet on the Small-Intestinal environment and mucosal integrity in the Gut-Liver axis. Cells 10: 3168, 2021.
28. Schroeder JA, Kuether EA, Fang J, Jing W, Weiler H, Wilcox DA, Montgomery RR and Shi Q: Thromboelastometry assessment of hemostatic properties in various murine models with coagulopathy and the effect of factor VIII therapeutics. J Thromb Haemost 19: 2417-2427, 2021.
29. Stacchiotti A, Ricci F, Rezzani R, Li Volti G, Borsani E, Lavazza A, Bianchi R and Rodella LF: Tubular stress proteins and nitric oxide synthase expression in rat kidney exposed to mercuric chloride and melatonin. J Histochem Cytochem 54: 1149-1157, 2006.
30. Phillippi DT, Daniel S, Nguyen KN, Penaredondo BA and Lund AK: Probiotics function as immunomodulators in the intestine in C57Bl/6 male mice exposed to inhaled diesel exhaust particles on a High-Fat diet. Cells 11: 1445, 2022.
31. Tizro P, Choi C and Khanlou N: Sample preparation for transmission electron microscopy. Methods Mol Biol 1897: 417-424, 2019.
32. Yan JT, Liu XY, Liu JH, Li GW, Zheng LF, Zhang XL, Zhang Y, Feng XY and Zhu JX: Reduced acetylcholine and elevated muscarinic receptor 2 in duodenal mucosa contribute to the impairment of mucus secretion in 6-hydroxydopamine-induced Parkinson's disease rats. Cell Tissue Res 386: 249-260, 2021.
33. Livak KJ and Schmittgen TD: Analysis of relative gene expression data using real-time quantitative PCR and the 2(-Delta Delta C(T)) method. Methods 25: 402-408, 2001.
34. Szymanska E, Szymanska S, Dadalski M and Kierkus J: Biological markers of disease activity in inflammatory bowel diseases. Prz Gastroenterol 18: 141-147, 2023.
35. Gurram PC, Manandhar S, Satarker S, Mudgal J, Arora D and Nampoothiri M: Dopaminergic signaling as a plausible modulator of astrocytic toll-like receptor 4: A crosstalk between neuroinflammation and cognition. CNS Neurol Disord Drug Targets 22: 539-557, 2023.

36. Dinarello CA: Interleukin-1 in the pathogenesis and treatment of inflammatory diseases. Blood 117: 3720-3732, 2011.
37. Brenner D, Blaser H and Mak TW: Regulation of tumour necrosis factor signalling: Live or let die. Nat Rev Immunol 15:362-374, 2015.
38. Grosheva I, Zheng D, Levy M, Polansky O, Lichtenstein A, Golani O, Dori-Bachash M, Moresi C, Shapiro H, Del Mare-Roumani S, *et al*: High-Throughput screen identifies host and microbiota regulators of intestinal barrier function. Gastroenterology 159: 1807-1823, 2020.
39. Melhem H, Regan-Komito D and Niess JH: Mucins dynamics in physiological and pathological conditions. Int J Mol Sci 22: 13642, 2021.
40. Okamoto R, Tsuchiya K, Nemoto Y, Akiyama J, Nakamura T, Kanai T and Watanabe M: Requirement of Notch activation during regeneration of the intestinal epithelia. Am J Physiol Gastrointest Liver Physiol 296: G23-G35, 2009.
41. Jankowsky JL, Slunt HH, Ratovitski T, Jenkins NA, Copeland NG and Borchelt DR: Co-expression of multiple transgenes in mouse CNS: A comparison of strategies. Biomol Eng 17: 157-165, 2001.
42. Garcia-Alloza M, Robbins EM, Zhang-Nunes SX, Purcell SM, Betensky RA, Raju S, Prada C, Greenberg SM, Bacskai BJ and Frosch MP: Characterization of amyloid deposition in the APPswe/PS1dE9 mouse model of Alzheimer disease. Neurobiol Dis 24: 516-524, 2006.
43. Duyckaerts C, Potier MC and Delatour B: Alzheimer disease models and human neuropathology: Similarities and differences. Acta Neuropathol 115: 5-38, 2008.
44. Turner JR: Intestinal mucosal barrier function in health and disease. Nat Rev Immunol 9: 799-809, 2009.
45. Choonara BF, Choonara YE, Kumar P, Bijukumar D, du Toit LC and Pillay V: A review of advanced oral drug delivery technologies facilitating the protection and absorption of protein and peptide molecules. Biotechnol Adv 32: 1269-1282, 2014.
46. Groschwitz KR and Hogan SP: Intestinal barrier function: Molecular regulation and disease pathogenesis. J Allergy Clin Immunol 124: 3-20, 2009.
47. Odenwald MA and Turner JR: The intestinal epithelial barrier: A therapeutic target? Nat Rev Gastroenterol Hepatol 14: 9-21, 2017.
48. Camilleri M: Leaky gut: Mechanisms, measurement and clinical implications in humans. Gut 68: 1516-1526, 2019.
49. Pellegrini C, Ippolito C, Segnani C, Dolfi A, Errede M, Virgintino D, Fornai M, Antonioli L, Garelli F, Nericcio A, *et al*: Pathological remodelling of colonic wall following dopaminergic nigrostriatal neurodegeneration. Neurobiol Dis 139: 104821, 2020.
50. Nighot P and Ma T: Endocytosis of intestinal tight junction proteins: In Time and Space. Inflamm Bowel Dis 27: 283-290, 2021.
51. Szczepanik AM, Rampe D and Ringheim GE. Amyloid-beta peptide fragments p3 and p4 induce pro-inflammatory cytokine and chemokine production in vitro and in vivo. J Neurochem 77: 304-317, 2001.
52. Zhou WW, Lu S, Su YJ, Xue D, Yu XL, Wang SW, Zhang H, Xu PX, Xie XX and Liu RT: Decreasing oxidative stress and neuroinflammation with a multifunctional peptide rescues memory deficits in mice with Alzheimer disease. Free Radic Biol Med 74: 50-63, 2014.
53. Fan Q, Liu Y, Wang X, Zhang Z, Fu Y, Liu L, Wang P, Ma H, Ma H, Seeram NP, *et al*: Ginnalin a inhibits aggregation, reverses fibrillogenesis, and alleviates cytotoxicity of amyloid β(1-42). ACS Chem Neurosci 11: 638-647, 2020.
54. Conway KL, Kuballa P, Song JH, Patel KK, Castoreno AB, Yilmaz OH, Jijon HB, Zhang M, Aldrich LN, Villablanca EJ, *et al*: Atg16l1 is required for autophagy in intestinal epithelial cells and protection of mice from Salmonella infection. Gastroenterology 145: 1347-1357, 2013.
55. Weiss GA, Grabinger T, Glaus Garzon J, Hasler T, Greppi A, Lacroix C, Khanzhin N and Hennet T: Intestinal inflammation alters mucosal carbohydrate foraging and monosaccharide incorporation into microbial glycans. Cell Microbiol 23: e13269, 2021.
56. De Gregorio V, Imparato G, Urciuolo F and Netti PA: Micro-patterned endogenous stroma equivalent induces polarized crypt-villus architecture of human small intestinal epithelium. Acta Biomater 81: 43-59, 2018.
57. McCaffrey C, Corrigan A, Moynagh P and Murphy R: Effect of yeast cell wall supplementation on intestinal integrity, digestive enzyme activity and immune traits of broilers. Br Poult Sci 62: 771-782, 2021.
58. Escande F, Porchet N, Bernigaud A, Petitprez D, Aubert JP and Buisine MP: The mouse secreted gel-forming mucin gene cluster. Biochim Biophys Acta 1676: 240-250, 2004.
59. Luis AS and Hansson GC: Intestinal mucus and their glycans: A habitat for thriving microbiota. Cell Host Microbe 31: 1087-100, 2023.
60. Muthupalani S, Ge Z, Joy J, Feng Y, Dobey C, Cho HY, Langenbach R, Wang TC, Hagen SJ and Fox JG: Muc5ac null mice are predisposed to spontaneous gastric antro-pyloric hyperplasia and adenomas coupled with attenuated H. pylori-induced corpus mucous metaplasia. Lab Invest 99: 1887-1905, 2019.
61. Higuchi R, Song C, Hoshina R and Suzaki T: Endosymbiosis-related changes in ultrastructure and chemical composition of Chlorella variabilis (Archaeplastida, Chlorophyta) cell wall in Paramecium bursaria (Ciliophora, Oligohymenophorea). Eur J Protistol 66: 149-155, 2018.
62. Papaspyropoulos A, Angelopoulou A, Mourkioti I, Polyzou A, Pankova D, Toskas K, Lanfredini S, Pantazaki AA, Lagopati N, Kotsinas A, *et al*: RASSF1A disrupts the NOTCH signaling axis via SNURF/RNF4-mediated ubiquitination of HES1. EMBO Rep 23: e51287, 2022.
63. Yagishita Y, Joshi T, Kensler TW and Wakabayashi N: Transcriptional Regulation of Math1 by Aryl Hydrocarbon Receptor: Effect on Math1+ Progenitor Cells in Mouse Small Intestine. Mol Cell Biol 43: 43-63, 2023.
64. Kim YS and Ho SB: Intestinal goblet cells and mucins in health and disease: Recent insights and progress. Curr Gastroenterol Rep 12: 319-330, 2010.
65. Shinoda M, Shin-Ya M, Naito Y, Kishida T, Ito R, Suzuki N, Yasuda H, Sakagami J, Imanishi J, Kataoka K, *et al*: Early-stage blocking of Notch signaling inhibits the depletion of goblet cells in dextran sodium sulfate-induced colitis in mice. J Gastroenterol 45: 608-617, 2010.
66. van der Flier LG and Clevers H: Stem cells, self-renewal, and differentiation in the intestinal epithelium. Annu Rev Physiol 71: 241-260, 2009.
67. Wu H, Chen QY, Wang WZ, Chu S, Liu XX, Liu YJ, Tan C, Zhu F, Deng SJ, Dong YL, *et al*: Compound sophorae decoction enhances intestinal barrier function of dextran sodium sulfate induced colitis via regulating notch signaling pathway in mice. Biomed Pharmacother 133: 110937, 2021.
68. Pope JL, Ahmad R, Bhat AA, Washington MK, Singh AB and Dhawan P: Claudin-1 overexpression in intestinal epithelial cells enhances susceptibility to adenamatous polyposis coli-mediated colon tumorigenesis. Mol Cancer 13: 167, 2014.
69. Pope JL, Bhat AA, Sharma A, Ahmad R, Krishnan M, Washington MK, Beauchamp RD, Singh AB and Dhawan P: Claudin-1 regulates intestinal epithelial homeostasis through the modulation of Notch-signalling. Gut 63: 622-634, 2014.
70. Battagin AS, Bertuzzo CS, Carvalho PO, Ortega MM and Marson FAL: Single nucleotide variants c.-13G → C (rs17429833) and c.108C → T (rs72466472) in the CLDN1 gene and increased risk for familial colorectal cancer. Gene 768: 145304, 2021.